



HAL
open science

Improvement of 3D mean field models for capillarity-driven grain growth based on full field simulations

Ludovic Maire, Benjamin Scholtes, Charbel Moussa, Nathalie Bozzolo, Daniel Pino Muñoz, Marc Bernacki

► **To cite this version:**

Ludovic Maire, Benjamin Scholtes, Charbel Moussa, Nathalie Bozzolo, Daniel Pino Muñoz, et al.. Improvement of 3D mean field models for capillarity-driven grain growth based on full field simulations. *Journal of Materials Science*, 2016, 51 (24), pp.10970-10981. 10.1007/s10853-016-0309-6 . hal-01369919

HAL Id: hal-01369919

<https://minesparis-psl.hal.science/hal-01369919>

Submitted on 16 May 2018

HAL is a multi-disciplinary open access archive for the deposit and dissemination of scientific research documents, whether they are published or not. The documents may come from teaching and research institutions in France or abroad, or from public or private research centers.

L'archive ouverte pluridisciplinaire **HAL**, est destinée au dépôt et à la diffusion de documents scientifiques de niveau recherche, publiés ou non, émanant des établissements d'enseignement et de recherche français ou étrangers, des laboratoires publics ou privés.

Improvement of 3-D mean field models for capillarity driven grain growth based on full field simulations

L.MAIRE · B.SCHOLTES · C.MOUSSA ·
N.BOZZOLO · D.PINO MUÑOZ · M.BERNACKI

Received: date / Accepted: date

Abstract In the present study, mean field models of grain growth (Hillert and Burke-Turnbull models) are compared with 3-D full field simulations considering an isotropic grain boundary energy and mobility and under the absence of second-phase particles. The present 3-D full field simulations are based on a level set description of the grain interfaces within a finite element framework. The digital initial microstructures are generated using a coupled "Voronoi-Laguerre/dense sphere packing" algorithm. Based on full field simulation results, new formulations of Burke-Turnbull and Hillert models are proposed. In contrast with classical formulations, the new ones account for the possible heterogeneity of the initial grain size distribution.

Keywords Grain growth · Mean field modeling · Full Field modeling · Level set

1 Introduction

Metallurgists have long observed that the macroscopic properties of the material, such as ductility, strength, thermal conductivity and hardness are strongly related to the microstructure, and especially to the mean grain size (R). Thus, understanding the phenomenon of grain growth (GG) occurring after recrystallization is crucial for the optimization of the microstructure and the final in-use properties of the material.

Single-phase fully dense polycrystals can generally be described by a log-normal grain size distribution (GSD) Fatima Vaz and Fortes (1988); Raeisinia and Sinclair (2009); Luther and Könke (2009), defined by (R) and a standard deviation (σ). The standard deviation is related to the width of the grain radius dispersion around (R). During grain growth mechanism, grain boundaries migrate under capillarity effects which results in an increase of (R)

L.MAIRE
MINES ParisTech, PSL - Research University, CEMEF - Centre de mise en forme des matériaux, CNRS UMR 7635, CS 10207 rue Claude Daunesse 06904 Sophia Antipolis Cedex, France.
Tel.: +33652693656
E-mail: ludovic.maire@mines-paristech.fr

B.SCHOLTES · C.MOUSSA · N.BOZZOLO · D.PINO MUÑOZ · M.BERNACKI
MINES ParisTech, PSL - Research University, CEMEF - Centre de mise en forme des matériaux, CNRS UMR 7635, CS 10207 rue Claude Daunesse 06904 Sophia Antipolis Cedex, France.

and σ . A previous study has highlighted that the heterogeneity in terms of GSD in the microstructure at the early stages of grain growth may have a first-order influence on the overall kinetics Cruz-Fabiano et al (2014), but this work was only based on 2-D considerations.

Macroscopic models, also called *mean field* (MF) models, are widely used to describe the grain growth kinetics, mainly due to their low computational cost. These models are based on empirical or semi-empirical laws and require experimental investigations to calibrate fitting parameters. Furthermore given that these models are most of the time based on average fields (mean radius and mean curvature), they are not adapted for capturing heterogeneous phenomena such as abnormal grain growth.

Thanks to the increase in computer performances, finer approaches called *full field* (FF) models have emerged in the last decades. These approaches consider a complete description of the microstructure topology at the polycrystal scale. A review of the most significant numerical methods is given in Hallberg (2011). Probabilistic voxel-based approaches such as *Monte Carlo* Rollett et al (1989); Rollett and Raabe (2001); Holm et al (2001) and *cellular automata* Raabe (1999) are very popular. Another approaches found in the literature is the *phase-field* Krill and Chen (2002) method, which offers the advantage of avoiding the difficult problem of tracking the interfaces. Finally, grain growth can also be modeled using a level set description of the interfaces within a finite element framework Bernacki et al (2008, 2011); Scholtes et al (2015); Hallberg (2013), which is the full field method used in this work.

In this study we propose to quantify the influence of the initial GSD in the context of 3-D grain growth. More specifically, the predictions of the Hillert Hillert (1965) and Burke-Turnbull (B&T) Burke and Turnbull (1952a) grain growth models are confronted with full field numerical simulations at the scale of a Representative Elementary Volume (REV) and under the assumptions of isotropic grain boundary energy and mobility, constant temperature and no precipitates. The digital initial microstructures are generated using a coupled "Voronoi-Laguerre/dense sphere packing" algorithm Hitti et al (2012); Hitti and Bernacki (2013).

2 Full field modeling of grain growth

2.1 Material parameters and numerical tools

A 5h heat treatment at a constant temperature of 1050°C for the austenitic 304L steel is simulated. Isotropic values are considered for the grain boundary mobility (M) and energy (γ). More precisely the product $M\gamma$ is fixed to $8.2 \times 10^{-7} \text{ J}\cdot\text{mm}^{-2}$, which is representative of a 304L stainless steel at 1050°C El Wahabi et al (2003); Cruz-Fabiano et al (2014). The material is assumed to be free of second phase particles (no Zener pinning effect).

The numerical simulations are performed on a cubic REV whose edge length varies from 2.00 to 2.85 mm. Each simulation was performed on 60 Intel Xeon CPUs. An unstructured mesh composed of 292^3 tetrahedral elements is used.

Eight different initial GSDs are considered to generate eight initial digital polycrystals. Each of them is defined by an initial mean grain radius (R_0) and standard deviation σ_0 . Their

characteristics are summarized in table 1 (line 1-4). The distributions LN_i with $i \in \{1, \dots, 7\}$ follow a log-normal distribution. The last one, referred to as BiM, is bimodal with modes $\lambda_1 = 50\mu\text{m}$ and $\lambda_2 = 100\mu\text{m}$. The initial number of grains in the REV is close to 8000 while at least 1200 grains remain at the end of the heat treatment (see Tab. 1 and Fig. 3). The REV dimensions, the time steps and the mesh size are chosen so as to justify a good convergence of results in terms of grain boundary kinetics Scholtes et al (2015, 2016).

		LN_1	LN_2	LN_3	LN_4	LN_5	LN_6	LN_7	BiM
Initial state ($t = 0\text{h}$)									
$\langle R_0 \rangle$	(μm)	62.0	66.0	74.3	75.3	82.2	89.4	99.0	75.2
σ_0	(μm)	6.90	11.8	19.4	7.50	25.9	30.9	17.7	25.5
$\ln(\sigma_0/\langle R_0 \rangle)$		-2.20	-1.71	-1.35	-2.30	-1.14	-1.05	-1.71	-1.08
No. Grains		7920	7576	7474	8100	7460	7636	7588	7472
Final state ($t = 5\text{h}$)									
$\langle R_f \rangle$	(μm)	109	120	135	111	151	160	138	115
σ_f	(μm)	39.0	45.0	53.2	39.8	59.9	66.3	50.7	36.0
$\ln(\sigma_f/\langle R_f \rangle)$		-1.03	-0.98	-0.93	-1.03	-0.92	-0.88	-1.00	-1.16
No. Grains		1483	1278	1244	2552	1221	1341	2803	2092

Table 1: Characteristics of the initial (lines 1-4) and final (lines 5-8) GSDs predicted by the full field simulations.

2.2 Full field simulation results

An histogram representing the instantaneous GSD is generated every minute of the heat treatment simulation. Each histogram is composed of 30 equally spaced intervals delimited by 0 and $300\mu\text{m}$. Next the term *distribution curve* is introduced to denote a linear approximation of a GSD histogram. The objective of these distribution curves is to simplify the representation of the GSDs for future comparisons. Fig. 1 provides a schematic illustration of the distribution curve obtained by piecewise linear approximation of an histogram.

The figure 2 shows all the distribution curves predicted by the full field simulations for every initial GSDs at the early (solid curves) and final (dashed curves) stages of the simulation. These will be confronted with the Hillert model predictions in the next section.

Table 1 (line 5-8) presents the characteristics of the final GSDs predicted by the full field simulations. The ratio $\ln(\sigma_f/\langle R_f \rangle)$ is observed to tend towards the value -1.00 after 5h of treatment for every initial GSD. The figure 3 illustrates several REV's of full field simulations at the beginning and at the end of the heat treatment, for the LN_1 and BiM initial GSDs. Among the REV's representing the log-normal GSDs, only the REV obtained for the LN_1 initial GSD is depicted since this latter is representative of all the log-normal initial GSDs. A preponderant blue color is observed at the beginning of the heat treatment for the LN_1 initial GSD, meaning that σ_0 is small for this distribution and most grains have sizes close to $\langle R_0 \rangle$. In the BiM initial GSD, two preponderant blue and green colors are observed in the REV at the beginning of the heat treatment. These two colors depict the two modes of the bimodal distribution, centered on grain size values of $50\mu\text{m}$ and $100\mu\text{m}$.

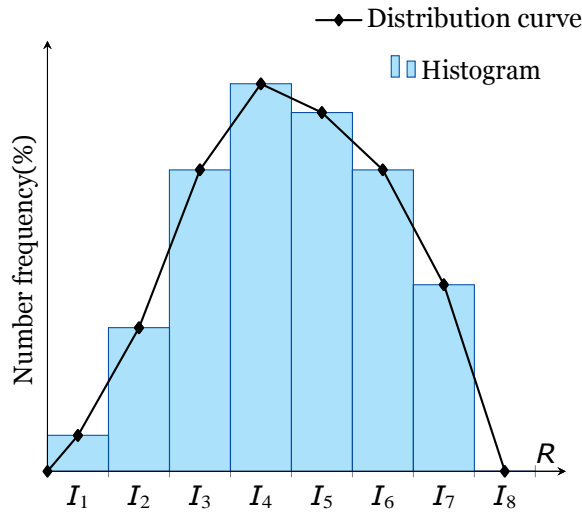


Fig. 1: Distribution curve obtained by linear approximation of an histogram

3 Confrontations of full field simulation results with Hillert model

3.1 Hillert model

In 1965, Hillert proposed a mean field model Hillert (1965) for normal grain growth. This model has already been discussed in many studies. Several authors, as in Darvishi Kamachali and Steinbach (2012); Darvishi Kamachali et al (2015); Suwa et al (2008); Rios et al (2006), recently confronted the predictions of this model with full field simulation results. Hillert model is considered to be more accurate than other grain growth models such as the one of B&T Burke and Turnbull (1952b), since it is based on a discrete representation of the microstructure. This discrete microstructure is composed of N classes of spherical grains having a radius R_i ($i \in \{1, \dots, N\}$). Each class of grains evolves according to the following equation:

$$\dot{R}_i = \beta M \gamma \left(\frac{1}{R_{cr}} - \frac{1}{R_i} \right), \quad (1)$$

where \dot{R}_i is the time derivative of R_i and R_{cr} is a critical grain radius. By applying the volume conservation in 3-D, it can be demonstrated that $R_{cr} = \sqrt{2} R$ Chao and Guoquan (2004); Rios et al (2006); Darvishi Kamachali et al (2015). For each initial GSD, the number of classes in the Hillert model has been taken equal to the number of grains in the REV of the corresponding full field simulation (see Tab. 1). The parameter β is a geometrical dimensionless constant which refers to the inherent approximations concerning the assumed idealized geometry in the Hillert model representation. In 3-D, β is assumed to be close to unity Hillert (1965). Other authors have nevertheless reported values above unity, such as $\beta \approx 1.25$ Darvishi Kamachali and Steinbach (2012) and $\beta \approx 1.1$ Suwa et al (2008). Darvishi

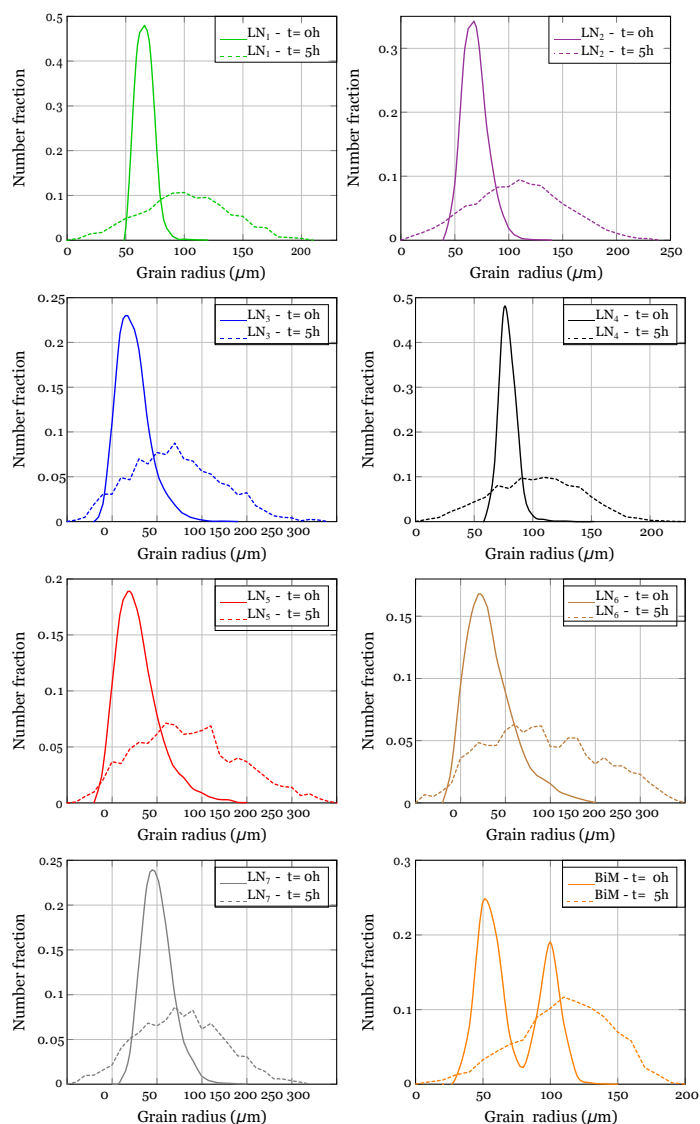


Fig. 2: Initial (solid curves) and final (dashed curves) distribution curves predicted by the full field simulations for the different initial GSDs.

Kamachali et al (2015) recently discussed a linear relationship valid in 3-D between the parameter β and the index $(R) \sqrt{R^2}$ which aims to account for the geometrical relations between the neighbourhood grains for any given initial distribution.

Hereafter, the notation $Hi(\beta)$ designates Eq. 1. So $Hi(1)$ corresponds to the classical Hillert formulation Hillert (1965). As it employs several grain classes, this model has the advantage of being able to predict the GSD evolution in addition to the (R) evolution. Previous works

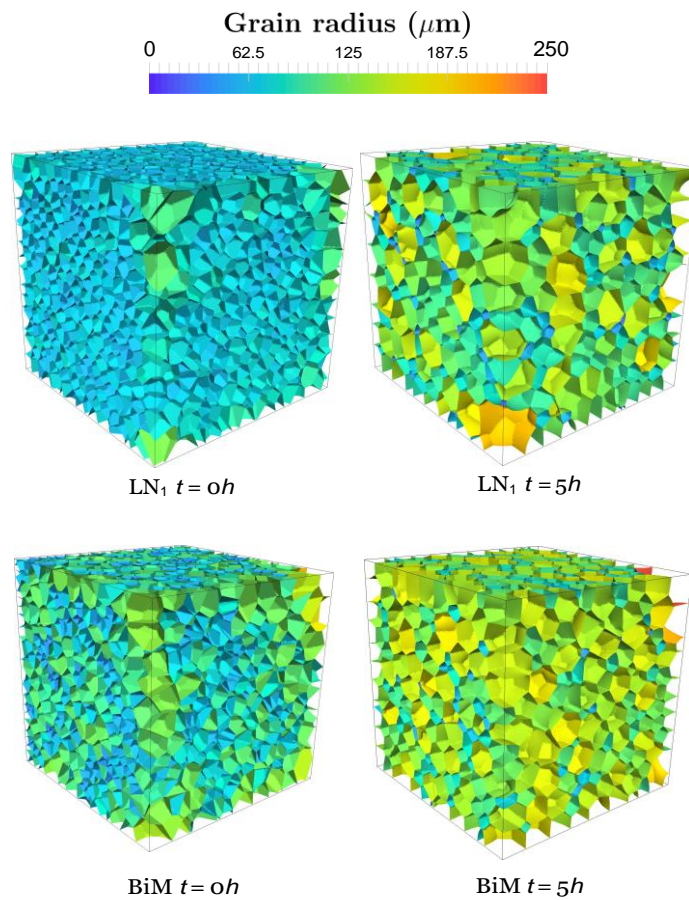


Fig. 3: Grain boundary networks at initial and final stages of the simulation for the LN₁ and BiM initial GSDs. The color code corresponds to the equivalent sphere radius of each grain.

have shown the ability of the classical Hillert model to correctly capture the grain growth kinetics in 2-D for different initial GSDs Cruz-Fabiano et al (2014). In the same manner as for full field simulations, a GSD histogram is generated every minute of the Hillert simulation. The distribution curves are then deduced from the GSD histograms according to the method illustrated on Fig. 1.

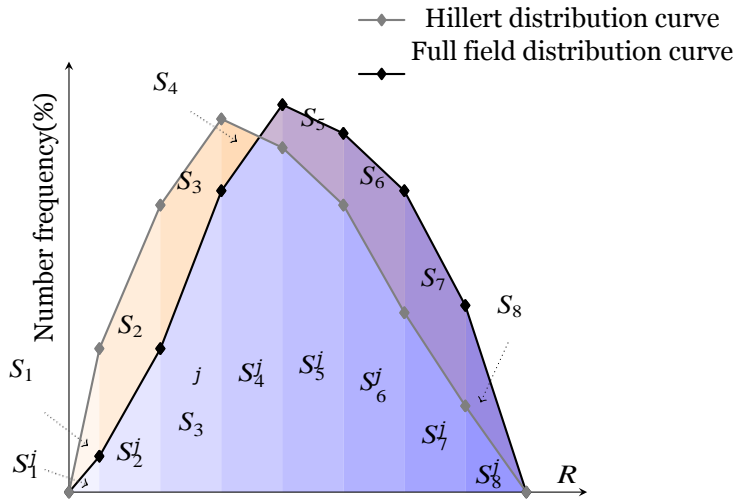


Fig. 4: Computed L^2_{Hi} error between the Hillert and full field distribution curve.

The notation L^2_{Hi} represents the instantaneous L^2 relative error measured between the distribution curves predicted by the Hillert and full field models. This quantity is computed as follows:

$$L^2_{Hi}(t) = 100 \times \frac{\sum_{i=1}^N (S_i - S_i^j)^2}{\sum_{i=1}^N (S_i^j)^2} \quad (2)$$

where, as illustrated on Fig. 4, the distributions are approximated by a linear interpolation and S_i (resp. S_i^j) denotes the area of the i -th obtained trapezoid under the Hillert (resp. the full field) distribution curve. Hereafter the notation (L^2_{Hi}) designates the time average of the $L^2_{Hi}(t)$ errors for a given simulation :

$$(L_{Hi}) = \frac{1}{N_{incr}} \sum L_{Hi}(t), \quad (3)$$

where N_{incr} is the number of time increments (equal to 300 in this study, $dt = 1min$).

3.2 Optimization of the Hillert model

The values of (L^2_{Hi}) errors obtained with the Hi(1) model are depicted by blue bars on Fig.5. This error remains globally constant around 20% for all the initial GSDs. These results confirm the versatility of this model although a difference of 26% is observed for the LN_4 and

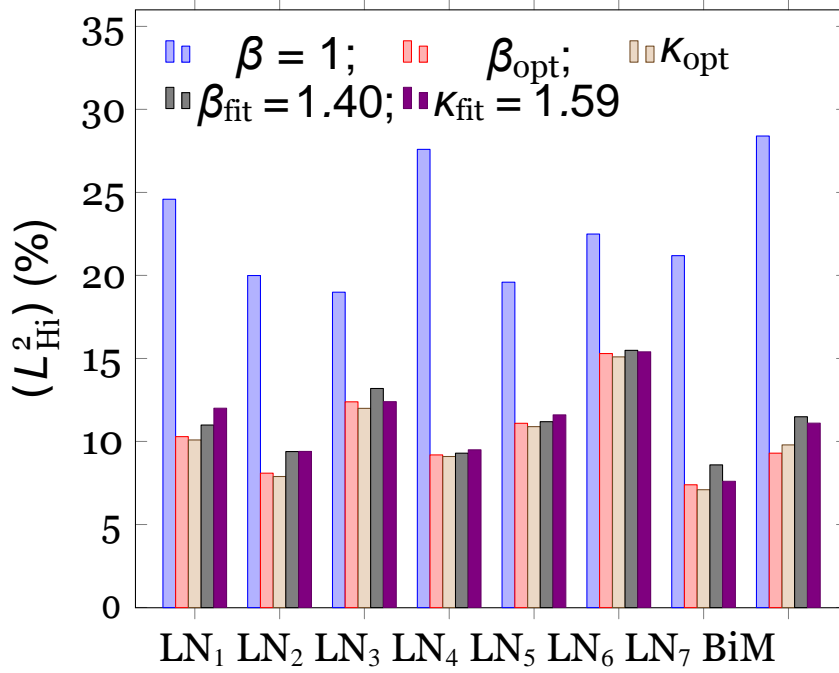


Fig. 5: Comparison in terms of (L^2) error on the distribution curves predicted by the full field and Hillert models (see Eq. 2 for details).

BiM initial GSDs. The distribution curves predicted by the Hi(1) (blue curves) and the FF model (red curves) are also compared at different stages of the heat treatment on Fig. 7. The kinetic of grain growth obtained with the Hillert model seems to be slower than that obtained with the FF model. This is observable on Fig. 7 at each instant of the simulation by a time shift of the Hillert distribution curves with respect to the full field distribution curves.

As stated above, the value $\beta = 1$ proposed by Hillert relies on many assumptions. For example Hillert consider that each shrinking grain has four immediate neighbours just before disappearing. Furthermore he considered that the β value is two times larger in 3-D than in 2-D where $\beta = 0.5$ according to Hillert Hillert (1965). Although these assumptions are judicious and justified, we propose to recalibrated this Hillert parameter based on the results of the full field simulations. Thus, several Hillert calculations have been performed by varying the beta value from 0.5 to 2 by step of 0.01. We denote β_{opt} the value of β in Eq. 1 that minimizes (L^2_{Hi}) error for each initial GSD. The values of β_{opt} are provided in Tab. 2. Red bars on Fig. 5 show the residual L^2_{Hi} error obtained with β_{opt} . These residual errors have approximately been reduced by half compared to the classical value of β equal to 1. Furthermore the values of β_{opt} are distributed around a mean value of 1.40 noted β_{fit} (see green dots on Fig.6).

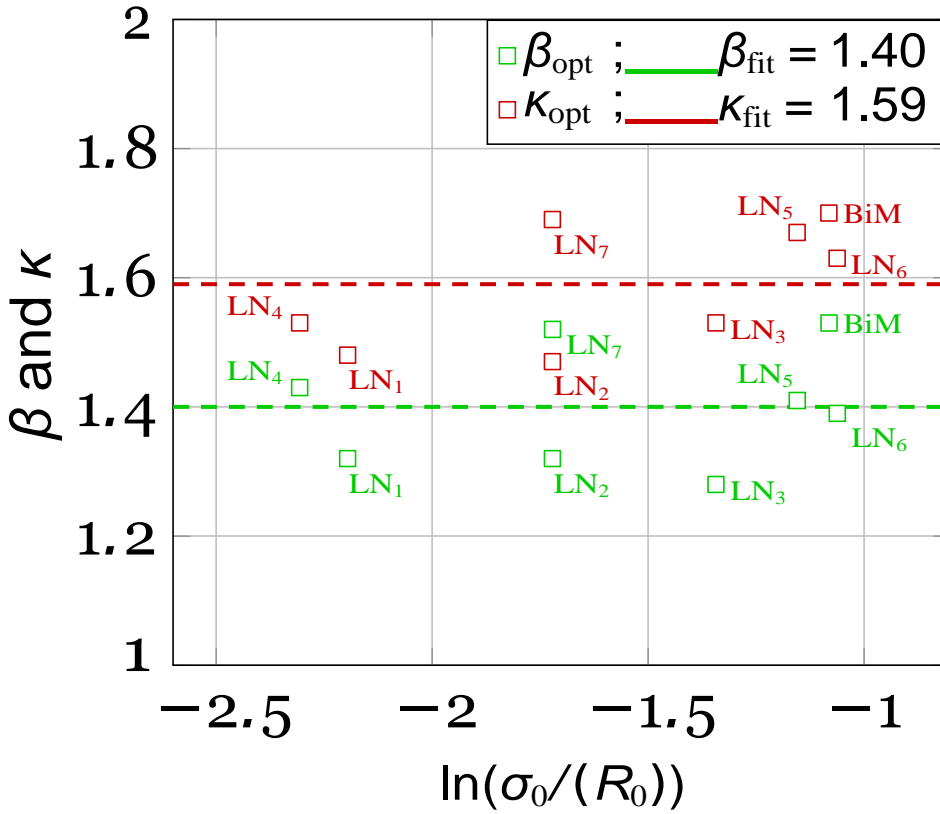


Fig. 6: Optimized values β_{opt} and κ_{opt} obtained by inverse analysis from the FF simulation results and fitting values β_{fit} and κ_{fit} obtained by an average of the optimized values.

To validate the calibrated value of $\beta = 1.40$, the distribution curves predicted by the Hi(1.40) (green curves) and the full field models (red curves) are compared at different stages of the heat treatment on Fig. 7. It is worth noting that Hi(1.40) model provides non negligible improvements for the prediction of the GSDs compared to the initial Hi(1) model. Indeed, the time shift observed Fig. 7 between full field and Hi(1) distribution curves has been now rectified since this new value of $\beta = 1.4$ is larger than the old one and thus logically increases the kinetic of grain growth. In a general way, the shapes of the GSDs are also in good agreement with the observation of Darvishi Kamachali and Steinbach (2012). GSDs are observed to be initially sharp and then become larger and larger during the heat treatment. After 2.5h of treatment in the BiM initial case, one single peak is observed on the distribution curve, which means that the two modes merge in the first hours of the heat treatment.

In order to investigate further the theory of Darvishi Kamachali et al (2015), we define κ_0 as :

$$\kappa_0 = \frac{\beta_{opt}}{(R)^2 / (R^2)_{(t=0)}}, \quad (4)$$

where the index $(R)/R^2$ is taken at the instant $t = 0s$ of the treatment. This choice has been done since this value does not significantly evolve during a simulation. The different values of κ_0 computed for every initial GSDs are provided in Line 3 of Tab. 2. These ratios are not constant between each initial GSDs, meaning that there is not a direct relation between β and the index $(R)/R^2$ for our cases. However this index, which considers the geometrical characteristics of neighbouring grains, could be useful to enrich the classical Hillert model (see Eq. 1).

Thus by replacing the β parameter in Eq. 1 by the product of an assumed constant parameter noted κ times the ratio $(R)/R^2$, we can consider the following Hillert model derived from the Darvishi Kamachali theory Darvishi Kamachali et al (2015) :

$$R_i = \kappa \frac{(R)^2}{(R^2)} M \gamma - \frac{1}{R_{cr}} - \frac{1}{R_i'} \quad (5)$$

where κ is a constant parameter. We performed several Hillert calculations using this new formulation (see Eq. 5) and by varying the κ value from 1 to 2 with a step of 0.01. We denote by κ_{opt} the value of κ that minimizes (L_{Hi}^2) for each initial GSD. The κ_{opt} values are presented in Line 4 of Tab. 2. Grey bars on Fig. 5 show the residual L_{Hi} error obtained with κ_{opt} . These residual errors are slightly little smaller than those obtained with β_{opt} . However this difference is not significant enough to affirm that the model given by Eq. 5 gives better predictions than Hi(1.4) model. Furthermore the κ_{opt} values are distributed around a mean value of 1.59 noted κ_{fit} (see red dots on Fig.6) resulting also in a low (L_{Hi}^2) error close to that obtained with the Hi(β_{fit}) model (see purple bars on Fig. 5). These similar errors are logically due to the fact that the Hi(1.4) (Eq. 1) and the new Hillert formulation (Eq. 5) give very close predictions since the index $(R)/R^2$ does not change much during all our simulations. Finally, the distributions curves obtained according to the new Hillert formulation all overlay with those obtained according to the Hi(1.4) model.

	LN ₁	LN ₂	LN ₃	LN ₄	LN ₅	LN ₆	LN ₇	BiM
β_{opt}	1.32	1.32	1.28	1.43	1.41	1.39	1.52	1.53
β_{fit}	1.40							
κ_0	1.35	1.36	1.38	1.43	1.57	1.58	1.57	1.72
κ_{opt}	1.48	1.47	1.53	1.53	1.67	1.63	1.69	1.7
κ_{fit}	1.59							

Table 2: (Line 1-2) Optimized Hillert model parameter β_{opt} calculated by inverse analysis from the full field simulation results (see eq. 1) and fitted Hillert model parameter β_{fit} obtained by averaging the values of β_{opt} . (Line 3) Values of κ_0 defined as the ratio between β_{opt} and the initial index $(R)/R^2$ at time = 0s of every simulation. (Line 4-5) Optimized κ values (κ_{opt}) calculated by inverse analysis from the full field simulation results (see eq. 5) and fitted κ value (κ_{fit}) obtained by averaging the values of κ_{opt} .

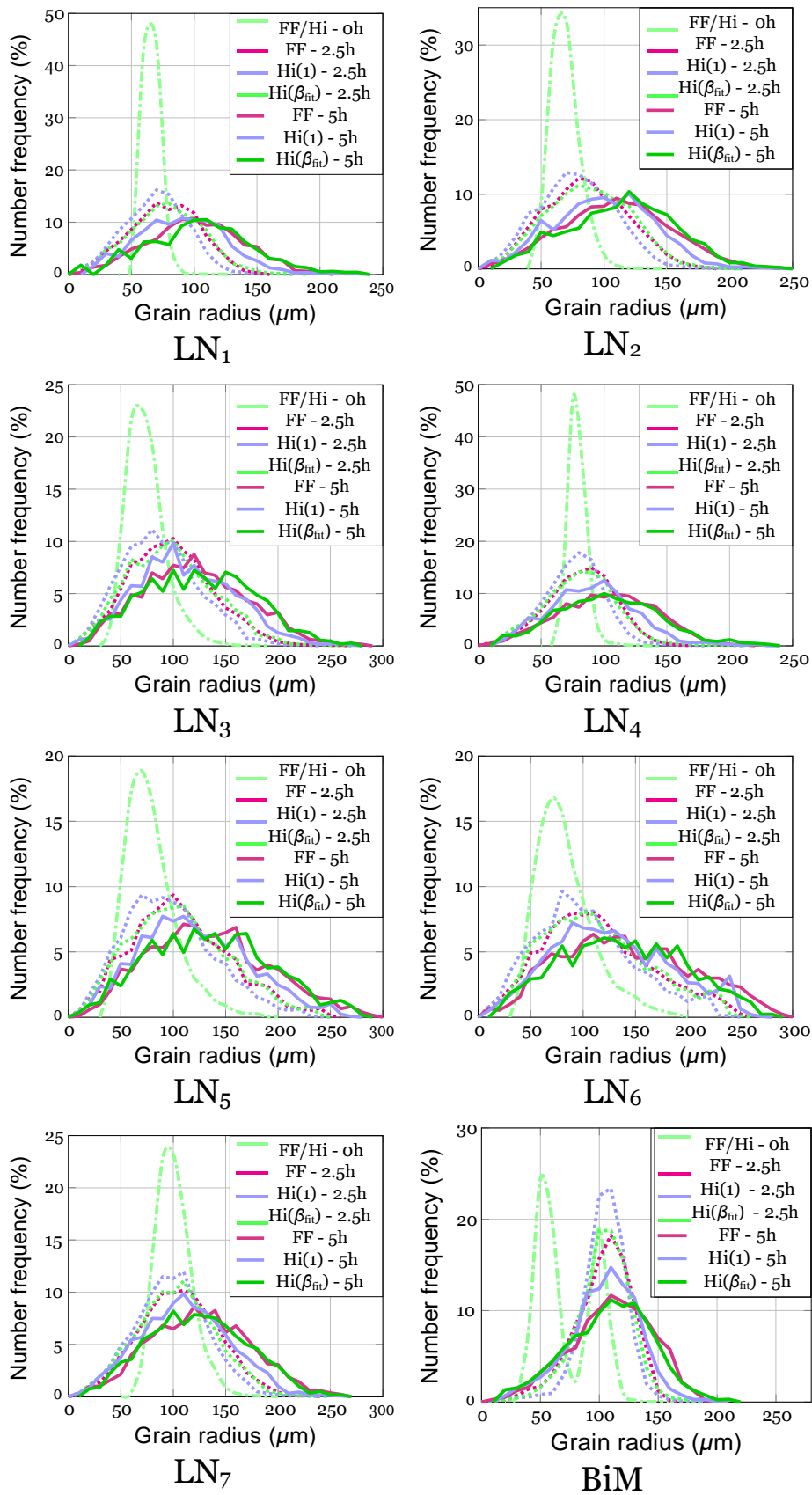


Fig. 7: Distribution curves predicted by the full field, Hi(1) and Hi(1.40) models for the different initial GSDs.

4 Confrontations of full field simulation results with B&T model

4.1 B&T model

For materials with a single mode and uniform grain size, describing the evolution of $R(t)$ could be sufficient as this quantity determines the global mechanical behavior of the material. Especially the Hall-Petch relationship states that the Yield stress of metallic materials can be expressed as a function of $R^{-0.5}$ Petch (1953). Furthermore in such cases, the initial GSD can be unknown and consequently the Hillert model can hardly be used. Thus, other mean field models can be used as a good alternative to describe the grain growth kinetics. In 1952, Burke and Turnbull (B&T) investigated the physical mechanisms of grain growth. They particularly assumed that grain boundaries migrate by atom transport toward their center of curvature, under a force due to their curved shape. These findings gave rise to the B&T model Burke and Turnbull (1952a), which predicts a parabolic evolution of R as a function of the time t :

$$(R)^2 - (R_0)^2 = \delta M \gamma t, \quad (6)$$

where $\delta = 0.5$ according to Burke and Turnbull (1952a); Darvishi Kamachali and Steinbach (2012). This analytic mean field model has the advantage of being extremely simple to use since it requires only a value for the product $(M\gamma)$ and for the initial mean grain size (R_0) .

The predictions of the B&T model will be confronted with the full field simulation results, using the following relative L^2 error:

$$L^2_{\text{B\&T}}(\%) = 100 \times \frac{\sum_{t=0}^{5h} ((R)_{\text{FF}}(t) - (R)_{\text{B\&T}}(t))^2}{\sum_{t=0}^{5h} (R)^2(t)}, \quad (7)$$

where $(R)_{\text{B\&T}}$ and $(R)_{\text{FF}}$ represent, respectively, the instantaneous values of R in the B&T and full field models.

4.2 New formulation of the B&T model

The resulting $L^2_{\text{B\&T}}$ measured between the classical B&T model predictions (Eq. 6) and the full field simulation results are illustrated by blue bars on Fig. 8. It is worth noting that these $L^2_{\text{B\&T}}$ are smaller than the (L^2_{Hi}) calculated in the previous section. Indeed $L^2_{\text{B\&T}}$ relies on a single quantity which is the mean grain size of the material. On the other hand (L^2_{Hi}) reflects the difference of shape between the two distribution curves. Results show that $L^2_{\text{B\&T}}$ is globally high for any initial case. Furthermore, $L^2_{\text{B\&T}}$ error globally increases when the ratio $\sigma_0/(R_0)$ decreases. This finding is actually quite logical and can be easily explained. Indeed in the case of small $\sigma_0/(R_0)$ ratios, the grain boundary kinetic slows down at the early stages of the treatment because most grains have a initial radius close to (R) . Consequently the increase of (R) takes longer to initiate and a plateau or even a decrease could be observed at

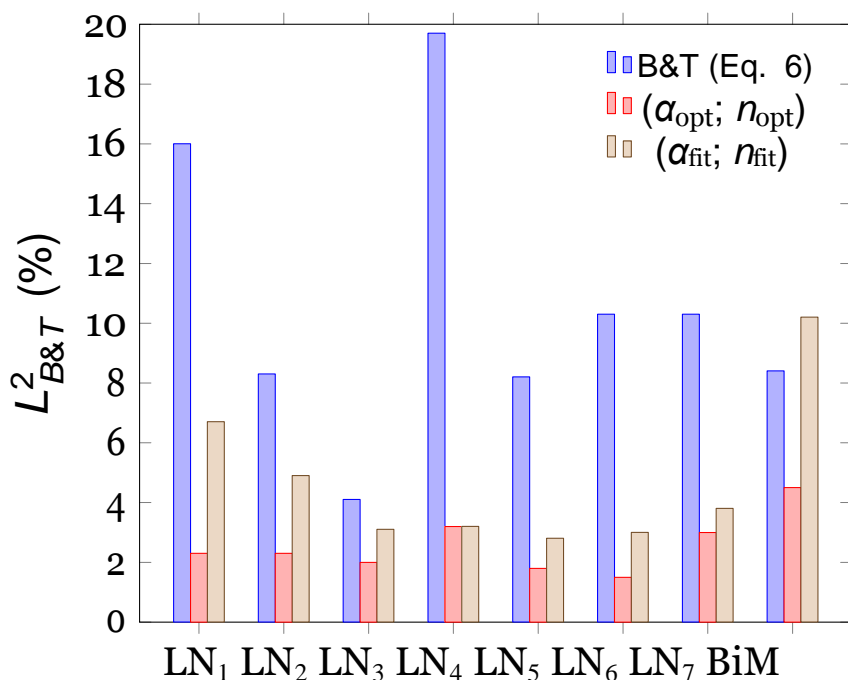


Fig. 8: Comparison in terms of L^2 error on the $\langle R \rangle$ values predicted by the full field simulations and the different B&T formulations (see Eq. 6 and Eq. 8 for more details).

the beginning of the thermal treatment. These typical evolutions occurring during the transient regime are not straightforward to capture with the classical B&T model. Furthermore given that the transient regime can last few hours in some initial configurations, it cannot be neglected by the models. These results confirm the interest of improving the classical B&T model. Recent numerical investigations in 2-D have also pointed out that B&T model is not accurate for every $\sigma_0/\langle R_0 \rangle$ initial ratios Cruz-Fabiano et al (2014).

In order to make the classical B&T formulation more accurate, the first objective is to determine whether there exists for each initial GSD, other δ values, noted δ_{opt} , that correctly describe the grain growth kinetics. These δ_{opt} values are obtained by minimizing the $L^2_{B\&T}$ for each initial GSD. The resulting fitting curves obtained by combining Eq. 6 and the δ_{opt} are depicted in Fig. 9 (dashed curves) for the LN₄ and LN₆ initial GSDs, which present the smallest and highest $\sigma_0/\langle R_0 \rangle$ ratios, respectively. It is observed that changing the values of δ does not correct the description of the transient regime. In particular for small $\sigma_0/\langle R_0 \rangle$ ratios, a model such as B&T model cannot be accurate enough to describe these particular mean grain size evolutions.

In order to also check the consistency of this law in the steady-state regime, the curves $\log(\langle R \rangle^2 - \langle R_0 \rangle^2) = f(\log(t))$ have been plotted on Fig. 10 according to full field results. A linear approximation of these curves is also added. We observed that the slopes of the linear

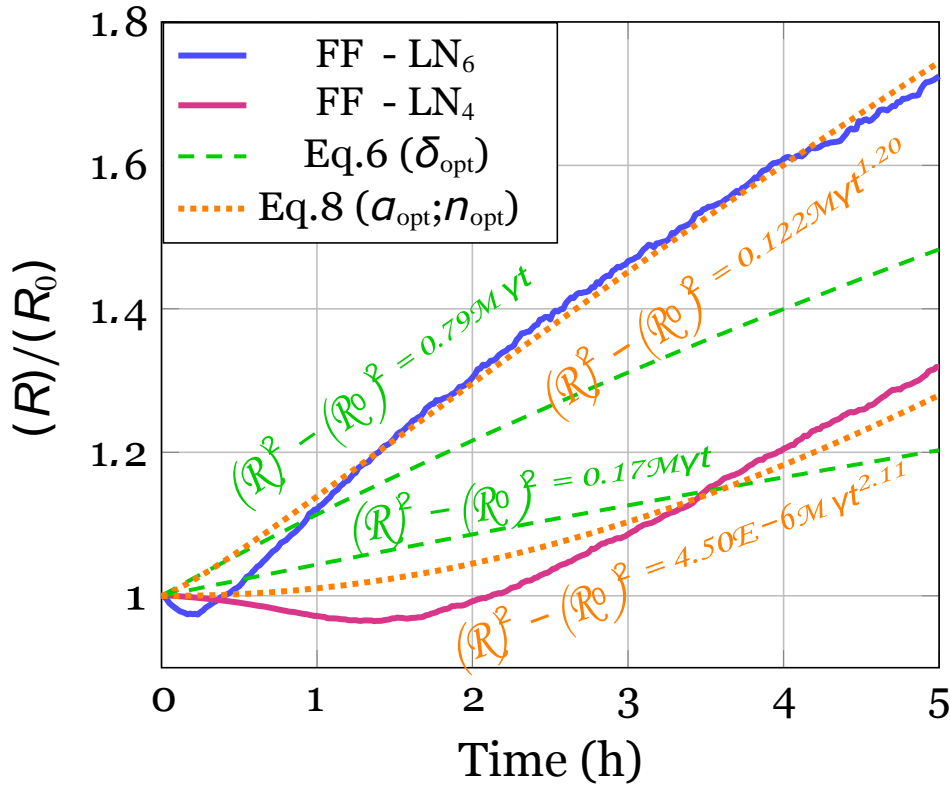


Fig. 9: Evolution of $(R)/R_0$ during the heat treatment. Solid curves corresponds to the full field results, dashed curves represent the B&T predictions obtained by combining Eq. 6 and δ_{opt} and dotted curves represent the B&T predictions obtained by combining Eq. 8 and the couple $(\alpha_{\text{opt}}; n_{\text{opt}})$.

approximations are quite different for every initial GSD as already observed in the work of Cruz-Fabiano et al (2014), which means that the classical B&T formulation cannot be sufficient to describe the kinetic of grain growth for every initial GSD.

Based on the previous observations, a new formulation of the B&T model has been proposed in Cruz-Fabiano et al (2014) including a new fitting exponent n aiming to take into account the different slopes observed on the Fig. 10 and the transient regimes observed on Fig. 9 :

$$(R)^2 - (R_0)^2 = \alpha M \gamma t^n, \quad (8)$$

where α is considered as a fitting parameter depending, in the same manner as the exponent n , on the initial GSD characteristics. Thus the validity of the classical B&T model (see Eq. (6)) can be easily verified if the slope n is equal to 1 and the fitted parameter α is equal to 0.5.

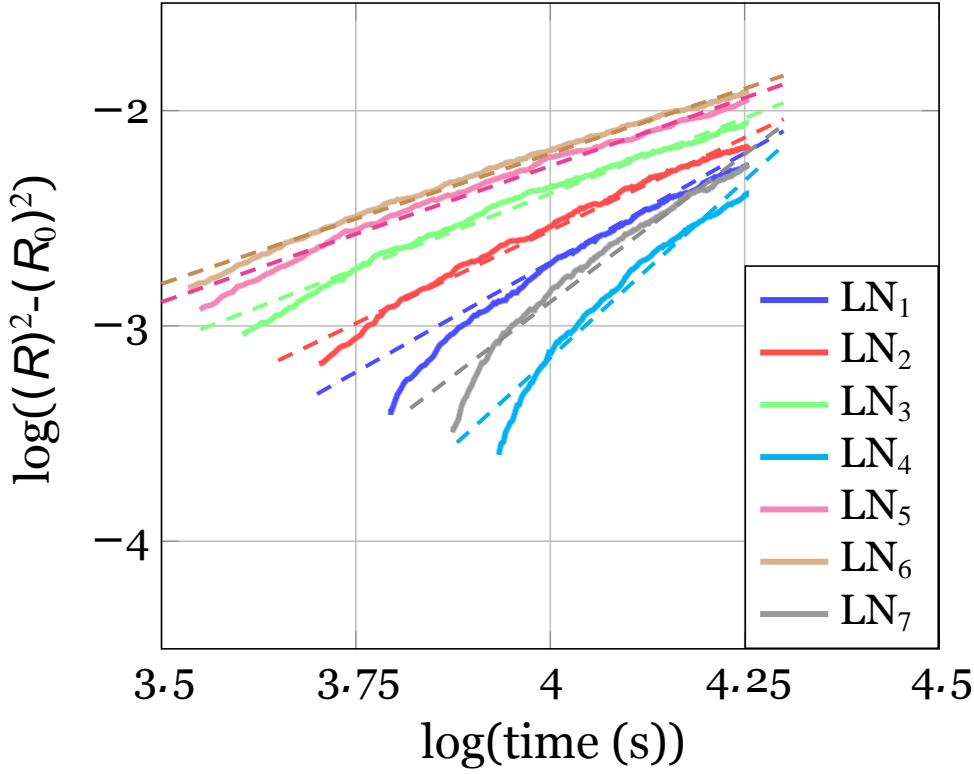


Fig. 10: Evolution of $\log((R)^2 - R_0^2)$ as a function of $\log(t)$ during the steady state regimes according to full field results. Linear approximations are added in dashed line.

	LN ₁	LN ₂	LN ₃	LN ₄	LN ₅	LN ₆	LN ₇	BiM
α_{opt}	6.20e-6	6.00e-4	1.66e-2	4.50e-6	7.45e-2	1.22e-1	6.18e-4	35.0
n_{opt}	2.13	1.69	1.37	2.11	1.24	1.20	1.64	0.56
α_{fit}	8.67e-6	5.67e-4	1.22e-2	3.69e-6	7.32e-2	1.58e-1	5.66e-4	1.22e-1
n_{fit}	2.06	1.67	1.39	2.13	1.23	1.16	1.67	1.18
$\ln(\sigma_0/(R_0))$	-2.20	-1.71	-1.35	-2.30	-1.14	-1.05	-1.71	-1.08

Table 3: (line 1-2) Optimized B&T model parameters α_{opt} and n_{opt} obtained by inverse analysis from the full field simulation results (see Eq. 6); (line 3-4) Fitted mean field model parameters α_{fit} and n_{fit} obtained by using the new formulations of Eq 9. (line 5) Ratio of the initial GSD characteristics.

Inverse analyses were performed in order to obtain optimal values of α_{opt} and n_{opt} which minimize $L_{\text{B\&T}}^2$. These values are plotted in Fig. 11 and the corresponding $L_{\text{B\&T}}^2$ are illustrated by red bars on Fig. 8. Interestingly, the results of Tab. 3 and Fig. 8 show that there exists, for each initial distribution, a set of parameters $(\alpha_{\text{opt}}; n_{\text{opt}})$ which predicts very accurately the evolution of (R) , with $L_{\text{B\&T}}^2 < 5\%$. Furthermore the LN₆ initial GSD presents the couple of parameters $(\alpha_{\text{opt}}; n_{\text{opt}})$ that is closest to the B&T classical parameters ($\alpha = 0.5; n = 1$). This distribution has the largest ratio $(\sigma_0/(R_0)) \approx 0.35$ of this study. It is worth

noting that increase the ratio σ_0/R_0 should lead to a new couple of parameters $(\alpha_{opt}; n_{opt})$ even closer to the B&T parameters. Cruz-Fabiano et al (2014) found in 2-D a couple parameters $(\alpha_{opt}; n_{opt})$ close to B&T parameters for initial GSDs having a ratio $\sigma_0/R_0 \approx 0.45$.

The predictions of (R) obtained by combining Eq. 8 with the set of parameters $(\alpha_{opt}; n_{opt})$ have been plotted on the Fig. 9 (dotted curves) for the LN₄ and LN₆ initial GSDs. It is clearly observed that the resulting curves obtained with Eq. 8 (dotted curves) are closer to full field predictions than resulting curves obtained with Eq. 6 (dashed curves). However, the transient regime characterized by a decrease in (R) during the first hour of treatment is not well described yet.

It is worth noting that the α_{opt} and the n_{opt} values increase and decrease respectively with the σ_0/R_0 ratio (see Tab. 3). This trend has already been observed in the study proposed by Cruz-Fabiano et al (2014). These observations confirm that the ratio σ_0/R_0 is relevant for describing the evolution of α and n . Furthermore, the sets of parameters $(\alpha_{opt}; n_{opt})$ are observed to be quasi identical for the two LN₂ and LN₇ initial GSDs which present the same σ_0/R_0 ratio. By plotting the parameters $\ln(\alpha_{opt})$ and n_{opt} as a function of the ratio $\ln(\sigma_0/R_0)$ on Fig 11, two linear relationships can be deduced for the n and α model parameters:

$$\ln(\alpha_{fit}) = 8.53 \ln \frac{\sigma_0}{R_0} + 7.11 \quad n_{fit} = -0.78 \ln \frac{\sigma_0}{R_0} + 0.34, \quad (9)$$

where these two constant parameters are quite different from those obtained in Cruz-Fabiano et al (2014) probably due to the fact that this study is investigated in 3-D. Combining Eq. 8 and Eq. 9 results in the following improved B&T formulation:

$$(R)^2 - (R_0)^2 = 1224.15 \frac{\sigma_0}{R_0} M\gamma t^{-0.78 \ln \frac{\sigma_0}{R_0} + 0.34}. \quad (10)$$

Although the set $(\ln(\alpha) = 3.56; n = 0.56)$ obtained for the BiM initial GSD predicts well the evolution of (R) , it does not follow the trends obtained for the log-normal initial GSDs (see Fig. 11). So the formulation of the B&T model given by Eq. 10 is only accurate for log-normal initial GSDs. By using $\alpha = \alpha_{fit}$ and $n = n_{fit}$ in Eq. 9 and 10, small $L_{B\&T}^2$ are obtained (see beige bars on Fig. 8 (b)). An interesting prospect of this study will be to perform the same analysis for different bimodal distributions.

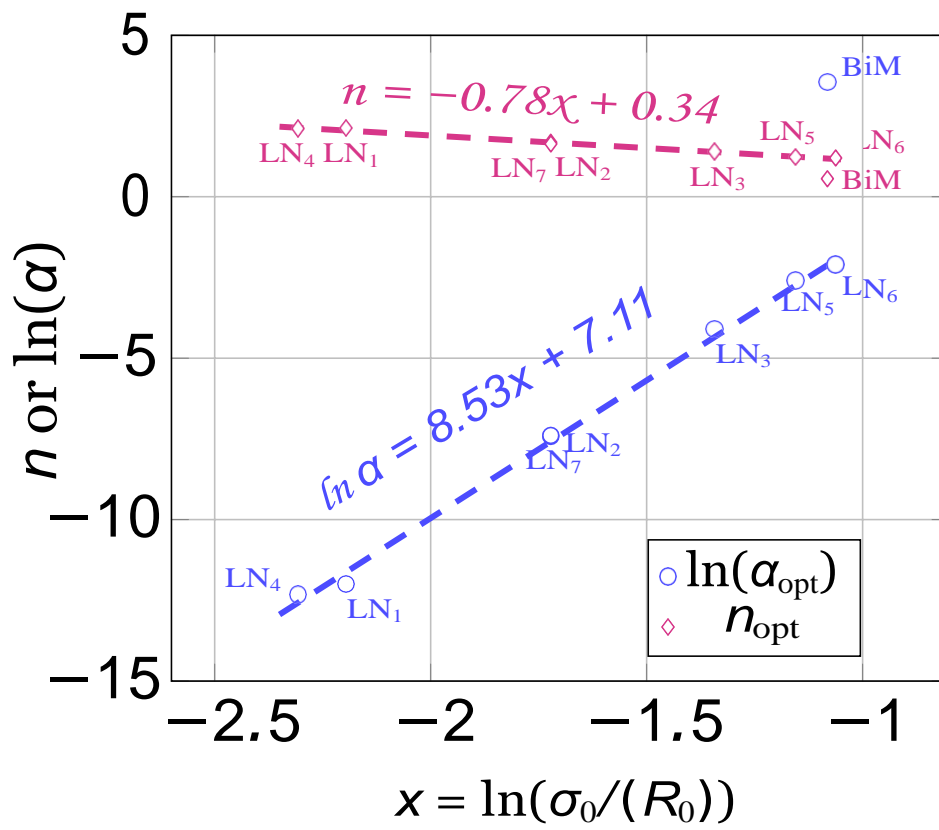


Fig. 11: Optimized values α_{opt} and n_{opt} obtained by inverse analysis from the FF simulation results and linear relationships between the set of parameters ($\ln(\alpha)$; n) and the ratio $\ln(\sigma_0/(R_0))$.

Conclusion

The present study is devoted to the modeling of ideal grain growth phenomenon. More specifically, the Hillert and B&T grain growth models have been confronted with large full field simulations at the polycrystal scale. These full field simulations are based on a level set method working within a finite element framework. Eight initial GSDs have been considered for the comparisons.

The Hillert model is shown to be versatile since it considers the initial GSD of the microstructure. However this model relies on a first-order parameter β which needs to be finely calibrated. Numerical full field investigations have highlighted a new value for β , which is globally constant around 1.4 for all initial distributions. We have finally demonstrated that the calibrated Hillert model predicts finely(R)and the evolution of the distribution curves, even for the BiM distribution.

The classical B&T model does not take into account the initial GSD, which makes it inaccurate in many cases. Based on full field simulation results, a new B&T formulation given in Eq. 9 has been proposed. This new formulation has been proven able to predict accurately the evolution of(R)for any log-normal initial GSD, regardless of σ_0 and(R_0). On the other hand, this new model is not universal and needs to be improved in order to consider other kinds of initial GSDs, like bimodal distributions.

Future work will be dedicated to (I) discuss the variability of the full field results obtained in comparison with the MacPherson-Srolovitz equation MacPherson and Srolovitz (2007) (II) perform additional simulations considering anisotropic grain boundary energy and/or mobility (III) complete the development of a full field model devoted to dynamic recrystallization (IV) perform the same kind of analysis in the context of the static and dynamic recrystallization phenomena (V) perform experimental measurements to be compared with the newly proposed mean field formulations.

Conflict of Interest: The authors declare that they have no conflict of interest.

References

- Abbruzzese G, Heckelmann I, Lücke K (1992) Statistical theory of two-dimensional grain growth. *Acta Metall Mater* 40(3):519–532
- Agnoli A, Bozzolo N, Loge´ RE, Franchet JM, Laigo J, Bernacki M (2014) Development of a level set methodology to simulate grain growth in the presence of real secondary phase particles and stored energy Application to a nickel-base superalloy. *Computational Materials Science* 89:233–241, DOI 10.1016/j.commatsci.2014.03.054, URL <http://linkinghub.elsevier.com/retrieve/pii/S0927025614002158>
- Aldina S, AC F, MA F (1985) Computer simulation of grain growth in a bidimensional polycrystal 19:1491–1496
- Beltran O, Huang K, Loge´ R (2015) A mean field model of dynamic and post-dynamic recrystallization predicting kinetics, grain size and flow stress. *Computational Materials Science* 102:293–303, DOI 10.1016/j.commatsci.2015.02.043, URL <http://linkinghub.elsevier.com/retrieve/pii/S0927025615001445>
- Bernacki M, Chastel Y, Coupez T, Loge´ R (2008) Level set framework for the numerical modelling of primary recrystallization in polycrystalline materials. *Scripta Materialia* 58(12):1129–1132,

- DOI 10.1016/j.scriptamat.2008.02.016, URL <http://linkinghub.elsevier.com/retrieve/pii/S1359646208001425>
- Bernacki M, Resk H, Coupez T, Loge RE (2009) Finite element model of primary recrystallization in polycrystalline aggregates using a level set framework. *Modelling and Simulation in Materials Science and Engineering* 17(6):064,006, DOI 10.1088/0965-0393/17/6/064006, URL <http://stacks.iop.org/0965-0393/17/i=6/a=064006?key=crossref.b10c4b90e783241fcb950f2c83e5932f>
- Bernacki M, Loge R, Coupez T (2011) Level set framework for the finite-element modelling of recrystallization and grain growth in polycrystalline materials. *Scripta Materialia* 64(6):525–528, DOI 10.1016/j.scriptamat.2010.11.032, URL <http://linkinghub.elsevier.com/retrieve/pii/S1359646210007906>
- Bernard P, Bag S, Huang K, Loge R (2011) A two-site mean field model of discontinuous dynamic recrystallization. *Materials Science and Engineering: A* 528(24):7357–7367, DOI 10.1016/j.msea.2011.06.023, URL <http://linkinghub.elsevier.com/retrieve/pii/S0921509311006757>
- Bulatov VV, Reed BW, Kumar M (2013) Grain boundary energy function for fcc metals. *Acta Materialia* 65:161–175, DOI 10.1016/j.actamat.2013.10.057, URL <http://dx.doi.org/10.1016/j.actamat.2013.10.057>
- Burke J, Turnbull D (1952a) Recrystallization and grain growth. *Prog Met Phys* 3:220
- Burke J, Turnbull D (1952b) Recrystallization and grain growth. *Progress in Metal Physics* 3:220–292, DOI 10.1016/0502-8205(52)90009-9
- Chao W, Guoquan LIU (2004) Reanalysis of the 3D quasi-stationary grain size distribution based on Hillert grain growth rate equation. *Ser E Technological Sciences* 47(1):112–120
- Chen F, Cui Z, Chen J (2014) Prediction of microstructural evolution during hot forging. *Manufacturing Review* 1:6, DOI 10.1051/mfreview/2014006, URL <http://mfr.edp-open.org/10.1051/mfreview/2014006>
- Cram DG, Zurob HS, Brechet YJM, Hutchinson CR (2009) Modelling discontinuous dynamic recrystallization using a physically based model for nucleation. *Acta Materialia* 57(17):5218–5228, DOI 10.1016/j.actamat.2009.07.024, URL <http://dx.doi.org/10.1016/j.actamat.2009.07.024>
- Cruz-Fabiano A, Loge R, Bernacki M (2014) Assessment of simplified 2D grain growth models from numerical experiments based on a level set framework. *Computational Materials Science* 92:305–312, DOI 10.1016/j.commatsci.2014.05.060, URL <http://linkinghub.elsevier.com/retrieve/pii/S0927025614003863>
- Darvishi Kamachali R, Steinbach I (2012) 3-D phase-field simulation of grain growth: Topological analysis versus mean-field approximations. *Acta Materialia* 60(6-7):2719–2728, DOI 10.1016/j.actamat.2012.01.037, URL <http://dx.doi.org/10.1016/j.actamat.2012.01.037>
- Darvishi Kamachali R, Abbondandolo A, Siburg KF, Steinbach I (2015) Geometrical grounds of mean field solutions for normal grain growth. *Acta Materialia* 90:252–258, DOI 10.1016/j.actamat.2015.02.025, URL <http://dx.doi.org/10.1016/j.actamat.2015.02.025>
- Dehghan-Manshadi A, Barnett M, Hodgson P (2008) Recrystallization in AISI 304 austenitic stainless steel during and after hot deformation. *Materials Science and Engineering: A* 485(1-2):664–672, DOI 10.1016/j.msea.2007.08.026, URL <http://linkinghub.elsevier.com/retrieve/pii/S0921509307015626>
- Ding R, Guo ZX (2001) Coupled quantitative simulation of microstructural evolution and plastic flow during dynamic recrystallization. *Acta Materialia* 49(16):3163–3175, DOI 10.1016/S1359-6454(01)00233-6
- El Wahabi M, Cabrera J, Prado J (2003) Hot working of two AISI 304 steels: a comparative study. *Materials Science and Engineering: A* 343(1-2):116–125, DOI 10.1016/S0921-5093(02)00357-X, URL <http://www.sciencedirect.com/science/article/pii/S092150930200357X>
- Elsay M, Esedoglu S, Smereka P (2011a) Large-scale simulations and parameter study for a simple recrystallization model. *Philosophical Magazine* 91(11):1607–1642, DOI 10.1080/14786435.2010.546377
- Elsay M, Esedoglu S, Smereka P (2011b) Large-scale simulation of normal grain growth via diffusion-generated motion. *Proceedings of the Royal Society A: Mathematical, Physical and Engineering Sciences* 467(2126):381–401, DOI 10.1098/rspa.2010.0194
- Esche S (2011) Monte Carlo Simulations of Grain Growth in Metals. *Applications of Monte Carlo Method in Science and Engineering (Cmc)*:581–610, DOI 10.5772/14942, URL http://cdn.intechopen.com/pdfs/14026/InTech-Monte_Carlo_simulations_of_grain_growth_in_metals.pdf
- Esedolu S (2016) Grain size distribution under simultaneous grain boundary migration and grain rotation in two dimensions. *Computational Materials Science* 121:209–216, DOI 10.1016/j.commatsci.2016.04.022, URL <http://linkinghub.elsevier.com/retrieve/pii/S0927025616301811>
- Fan XG, Yang H, Sun ZC, Zhang DW (2010) Quantitative analysis of dynamic recrystallization behavior using a grain boundary evolution based kinetic model. *Materials Science & Engineering A*

- 527(21-22):5368–5377, DOI 10.1016/j.msea.2010.05.032, URL <http://dx.doi.org/10.1016/j.msea.2010.05.032>
- Fatima Vaz M, Fortes M (1988) Grain size distribution : The lognormal and the gamma distribution functions. Pergamon journals 22:35–40
- Favre J, Fabrègue D, Chiba A, Bréchet Y (2013) Nucleation of recrystallization in fine-grained materials: an extension of the BaileyHirsch criterion. Philosophical Magazine Letters 93(11):631–639, DOI 10.1080/09500839.2013.833352, URL <http://www.tandfonline.com/doi/abs/10.1080/09500839.2013.833352>
- Hallberg H (2011) Approaches to Modeling of Recrystallization. Metals 1(1):16–48, DOI 10.3390/met1010016, URL <http://www.mdpi.com/2075-4701/1/1/16/>
- Hallberg H (2013) A modified level set approach to 2D modeling of dynamic recrystallization. Modelling and Simulation in Materials Science and Engineering 21(8):085,012, DOI 10.1088/0965-0393/21/8/085012, URL <http://stacks.iop.org/0965-0393/21/i=8/a=085012?key=crossref.fc2d86d9805f0075a83535b0524735cb>
- Hallberg H, Wallin M, Ristinmaa M (2010) Simulation of discontinuous dynamic recrystallization in pure Cu using a probabilistic cellular automaton. Computational Materials Science 49(1):25–34, DOI 10.1016/j.commatsci.2010.04.012, URL <http://linkinghub.elsevier.com/retrieve/pii/S0927025610002259>
- Hillert M (1965) On the theory of normal and abnormal grain growth. Acta Metall Mater 13:227, DOI 10.1017/CBO9781107415324.004, arXiv:1011.1669v3
- Hitti K, Bernacki M (2013) Optimized Dropping and Rolling (ODR) method for packing of poly-disperse spheres. Applied Mathematical Modelling 37(8):5715–5722, DOI 10.1016/j.apm.2012.11.018, URL <http://dx.doi.org/10.1016/j.apm.2012.11.018>
- Hitti K, Laure P, Coupez T, Silva L, Bernacki M (2012) Precise generation of complex statistical Representative Volume Elements (RVEs) in a finite element context. Computational Materials Science 61:224–238, DOI 10.1016/j.commatsci.2012.04.011, URL <http://dx.doi.org/10.1016/j.commatsci.2012.04.011>
- Holm EA, Hassold GN, Miodownik MA (2001) On misorientation distribution evolution during anisotropic grain growth. Acta Materialia 49(15):2981–2991, DOI 10.1016/S1359-6454(01)00207-5
- Jafari M, Najafizadeh A (2009) Correlation between Zener Hollomon parameter and necklace DRX during hot deformation of 316 stainless steel. Materials Science and Engineering 501:16–25, DOI 10.1016/j.msea.2008.09.073
- Jonas JJ, Queleñec X, Jiang L (2009) The Avrami kinetics of dynamic recrystallization. Acta Materialia 57:2748–2756, DOI 10.1016/j.actamat.2009.02.033
- Khoddam S, Hodgson P, Beladi H (2015) Computational inverse analysis of static recrystallization kinetics. International Journal of Mechanical Sciences 103:97–103, DOI 10.1016/j.ijmecsci.2015.09.008, URL <http://linkinghub.elsevier.com/retrieve/pii/S0020740315003264>
- Kim BN, Hiraga K, Morita K (2004) Kinetics of normal grain growth depending on the size distribution of small grains. Nippon Kinzoku Gakkaishi/Journal of the Japan Institute of Metals 68(10):913–918, DOI 10.2320/matertrans.44.2239
- Kim Si, Yoo Yc (2001) Dynamic recrystallization behavior of AISI 304 stainless steel. Materials Science and Engineering 311:108–113
- Krill CE, Chen LQ (2002) Computer simulation of 3-D grain growth using a phase-field model. Acta Materialia 50(12):3059–3075, DOI 10.1016/S1359-6454(02)00084-8, URL <http://www.sciencedirect.com/science/article/B6TW8-466R5TY-1/2/4e83847503c9ca5646b71d4de608f2fa>
- Lazar EA, Mason JK, MacPherson RD, Srolovitz DJ (2011) A more accurate three-dimensional grain growth algorithm. Acta Materialia 59(17):6837–6847, DOI 10.1016/j.actamat.2011.07.052, URL <http://dx.doi.org/10.1016/j.actamat.2011.07.052>
- Li X, Duan L, Li J, Wu X (2015) Experimental study and numerical simulation of dynamic recrystallization behavior of a micro-alloyed plastic mold steel. Materials and Design 66:309–320, DOI 10.1016/j.matdes.2014.10.076, URL <http://dx.doi.org/10.1016/j.matdes.2014.10.076>
- Lin Y, Chen XM (2011) A critical review of experimental results and constitutive descriptions for metals and alloys in hot working. Materials & Design 32(4):1733–1759, DOI 10.1016/j.matdes.2010.11.048, URL <http://www.sciencedirect.com/science/article/pii/S0261306910006746>
- Lücke K, Brandt R (1998) Normal and Abnormal Grain Growth as Transient Phenomena 6:67–76
- Lücke K, Heckelmann I, Abbruzzese G (1992) Statistical theory of two-dimensional grain growth II. Kinetics of grain growth. Acta Metallurgica et Materialia 40(3):533–542, DOI 10.1016/0956-7151(92)90402-Z, URL <http://www.sciencedirect.com/science/article/pii/095671519290402Z>
- Luther T, Könke C (2009) Polycrystal models for the analysis of intergranular crack growth in metallic materials. Engineering Fracture Mechanics 76(15):2332–2343, DOI 10.1016/j.engfracmech.2009.07.006,

- URL <http://dx.doi.org/10.1016/j.engfracmech.2009.07.006>
- MA (1939) Kinetics of Phase Change I-III. *J Chem Physics* 7:1103–1112
- MacPherson RD, Srolovitz DJ (2007) The von Neumann relation generalized to coarsening of three-dimensional microstructures. *Nature* 446(7139):1053–1055, DOI 10.1038/nature05745
- Madej L, Sitko M, Pietrzyk M (2016) Perceptive comparison of mean and full field dynamic recrystallization models. *Archives of Civil and Mechanical Engineering* 16(4):569–589, DOI 10.1016/j.acme.2016.03.010, URL <http://linkinghub.elsevier.com/retrieve/pii/S1644966516300115>
- Miodownik Ma (2002) A review of microstructural computer models used to simulate grain growth and recrystallisation in aluminium alloys. *Journal of Light Metals* 2(3 SPEC.):125–135, DOI 10.1016/S1471-5317(02)00039-1
- Mirzadeh H (2015) Constitutive modeling and prediction of hot deformation flow stress under dynamic recrystallization conditions. *Mechanics of Materials* 85:66–79, DOI 10.1016/j.mechmat.2015.02.014, URL <http://linkinghub.elsevier.com/retrieve/pii/S0167663615000617>
- Momeni A, Dehghani K, Ebrahimi GR (2011) Modeling the initiation of dynamic recrystallization using a dynamic recovery model. *Journal of Alloys and Compounds* 509(39):9387–9393, DOI 10.1016/j.jallcom.2011.07.014, URL <http://dx.doi.org/10.1016/j.jallcom.2011.07.014>
- Montheillet F, Lurdos O, Damamme G (2009) A grain scale approach for modeling steady-state discontinuous dynamic recrystallization. *Acta Materialia* 57(5):1602–1612, DOI 10.1016/j.actamat.2008.11.044, URL <http://linkinghub.elsevier.com/retrieve/pii/S1359645408008641>
- Olmsted DL, Holm EA, Foiles SM (2009) Survey of computed grain boundary properties in face-centered cubic metals II: Grain boundary mobility. *Acta Materialia* 57(13):3704–3713, DOI 10.1016/j.actamat.2009.04.015, URL <http://www.sciencedirect.com/science/article/pii/S1359645409002316>
- Petch N (1953) The cleavage strength of polycrystals. *J Iron Steel Inst* 174:25
- Piekos K, Tarasiuk J, Wierzbanski K, Bacroix B (2008) Generalized vertex model of recrystallization - Application to polycrystalline copper. *Computational Materials Science* 42(4):584–594, DOI 10.1016/j.commatsci.2007.09.014
- Raabe D (1999) Introduction of a scalable three-dimensional cellular automaton with a probabilistic switching rule for the discrete mesoscale simulation of recrystallization phenomena. *Philosophical Magazine A* 79(10):2339–2358, DOI 10.1080/01418619908214288, URL <http://www.tandfonline.com/doi/abs/10.1080/01418619908214288>
- Raeisinia B, Sinclair CW (2009) A representative grain size for the mechanical response of polycrystals. *Materials Science and Engineering A* 525(1-2):78–82, DOI 10.1016/j.msea.2009.06.045
- Rios PR, Dalpian TG, Brandao VS, Castro JA, Oliveira ACL (2006) Comparison of analytical grain size distributions with three-dimensional computer simulations and experimental data. *Scripta Materialia* 54(9):1633–1637, DOI 10.1016/j.scriptamat.2006.01.007
- Rollett AD (1997) Overview of modeling and simulation of recrystallization. *Progress in Materials Science* 42(1-4):79–99, DOI 10.1016/S0079-6425(97)00008-X
- Rollett AD, Raabe D (2001) A hybrid model for mesoscopic simulation of recrystallization. *Computational Materials Science* 21(1):69–78, DOI 10.1016/S0927-0256(00)00216-0, URL <http://www.sciencedirect.com/science/article/pii/S0927025600002160>
- Rollett AD, Srolovitz DJ, Anderson MP (1989) Simulation and theory of abnormal grain growth-anisotropic grain boundary energies and mobilities. *Acta Metallurgica* 37(4):1227–1240, DOI 10.1016/0001-6160(89)90117-X
- Roucoules C, Pietrzyk M, Hodgson PD (2003) Analysis of work hardening and recrystallization during the hot working of steel using a statistically based internal variable model. *Materials Science and Engineering A* 339(1-2):1–9, DOI 10.1016/S0921-5093(02)00120-X
- Sakai T, Belyakov A, Kaibyshev R, Miura H, Jonas JJ (2014) Dynamic and post-dynamic recrystallization under hot, cold and severe plastic deformation conditions. *Progress in Materials Science* 60:130–207, DOI 10.1016/j.pmatsci.2013.09.002, URL <http://linkinghub.elsevier.com/retrieve/pii/S0079642513000698>
- Scholtes B, Shakoor M, Settefrati A, Bouchard PO, Bozzolo N, Bernacki M (2015) New finite element developments for the full field modeling of microstructural evolutions using the level-set method. *Computational Materials Science* 109:388–398, DOI 10.1016/j.commatsci.2015.07.042, URL <http://linkinghub.elsevier.com/retrieve/pii/S0927025615004528>
- Scholtes B, Boulais-sinou R, Settefrati A, Pino Muñoz D, Poitraul I, Montouchet A, Bozzolo N, Bernacki M (2016) 3D level set modeling of static recrystallization considering stored energy fields. *Computational Materials Science*
- Shakoor M, Scholtes B, Bouchard PO, Bernacki M (2015) An efficient and parallel level set reinitialization method Application to micromechanics and microstructural evolutions. *Applied Mathematical Modelling* DOI 10.1016/j.apm.2015.03.014, URL <http://linkinghub.elsevier.com/retrieve/pii/>

- S0307904X15001638
- Suwa Y, Saito Y, Onodera H (2008) Parallel Computer Simulation of Three-Dimensional Grain Growth Using the Multi-Phase-Field Model. *Materials Transactions* 49(4):704–709, DOI 10.2320/matertrans.MRA2007225
- Tan K, Li J, Guan Z, Yang J, Shu J (2015) The identification of dynamic recrystallization and constitutive modeling during hot deformation of Ti55511 titanium alloy. *Materials & Design* 84:204–211, DOI 10.1016/j.matdes.2015.06.093, URL <http://linkinghub.elsevier.com/retrieve/pii/S0264127515004438>
- Zhao HK, Chan T, Merriman B, Osher S (1996) A Variational Level Set Approach to Multiphase Motion. *Journal of Computational Physics* 127(1):179–195, DOI 10.1006/jcph.1996.0167, URL <http://www.sciencedirect.com/science/article/pii/S0021999196901679>
- Zhao P, Song En Low T, Wang Y, Niezgoda SR (2016) An integrated full-field model of concurrent plastic deformation and microstructure evolution: Application to 3D simulation of dynamic recrystallization in polycrystalline copper. *International Journal of Plasticity* 80:38–55, DOI 10.1016/j.ijplas.2015.12.010, URL <http://dx.doi.org/10.1016/j.ijplas.2015.12.010>, 1509.04953
- Zhu R, Liu Q, Li J, Xiang S, Chen Y, Zhang X (2015) Dynamic restoration mechanism and physically based constitutive model of 2050 Al e Li alloy during hot compression. *Journal of Alloys and Compounds* 650:75–85, DOI 10.1016/j.jallcom.2015.07.182, URL <http://dx.doi.org/10.1016/j.jallcom.2015.07.182>
- Zouari M, Bozzolo N, Loge RE (2016) Mean field modelling of dynamic and post-dynamic recrystallization during hot deformation of Inconel 718 in the absence of δ phase particles. *Materials Science and Engineering: A* 655:1–17, DOI 10.1016/j.msea.2015.12.102, URL <http://linkinghub.elsevier.com/retrieve/pii/S0921509315307930>
- Zurob H, Brechet Y, Dunlop J (2006) Quantitative criterion for recrystallization nucleation in single-phase alloys: Prediction of critical strains and incubation times. *Acta Materialia* 54(15):3983–3990, DOI 10.1016/j.actamat.2006.04.028, URL <http://linkinghub.elsevier.com/retrieve/pii/S1359645406003181>